RESEARCH ARTICLE

polymers advanced technologies   WILEY

Electro-responsive shape-memory composites obtained via dual-curing processing

Claudio Russo[1] | José Luis Ramírez[2] | Xavier Fernández-Francos[3] | Silvia De la Flor[1]

[1]Department of Mechanical Engineering, Universitat Rovira i Virgili, Tarragona, Spain

[2]Department of Electrical, Electronic, Engineering and Automation, Universitat Rovira i Virgili, Tarragona, Spain

[3]Thermodynamics Laboratory, ETSEIB, Universitat Politècnica de Catalunya, Barcelona, Spain

Correspondence
Xavier Fernández-Francos and Silvia De la Flor, Department of Mechanical Engineering, Universitat Rovira i Virgili, Tarragona, Spain.
Email: xavier.fernandez@upc.edu; silvia.delaflor@urv.cat

Abstract

In this work, electro-responsive shape-memory actuators were developed by incorporating a conductive heater in a dual-curing thiol-acrylate-epoxy shape-memory polymer (SMP). A conductive heater, consisting of an electrically conductive silver-ink track printed on Kapton® substrate, was assembled to the SMP, taking advantage of the dual-curing processing. The shape-memory effect (SME) was activated by the heat dissipated by the Joule effect in the conductive track. Boron nitride agglomerates were dispersed in the thiol-acrylate-epoxy layers to increase thermal conductivity and achieve faster shape-recovery. A thermoelectric control unit was developed to control the shape recovery of the electro-responsive actuators and provide different activation strategies. The electrically activated SME was investigated and compared to a traditional SME based on an external heating source given by the dynamic mechanical analyzer (DMA) apparatus. Electro-responsive actuators were found extremely faster than the conventional SMPs based on external heating. The fastest recovery was obtained by the 15% boron nitride actuator, which recovered the 100% of the original shape in only 8 s. The thermoelectric controlling device provided an optimal control of the shape recovery speed based on the pulse width modulation of the heating current under the application of a low voltage (5 V).

KEYWORDS
conductive heater, dual-curing, electro-responsive actuators, shape-memory polymers

1 | INTRODUCTION

Shape-memory polymers (SMPs) are a class of stimuli-responsive materials that are able to change shape in response to an external stimulus.[1,2] The shape memory effect (SME) consists of recovering a permanent shape triggered by external stimuli such as heating, electromagnetic field, light, or vapor. SMPs found a wide range of applications which is ever wider thanks to the progress and design of more advanced polymeric materials: from biomedical applications,[3–5] through self-morphing and self-deploying structures in aviation,[6] to smart open-closing mechanisms in industrial applications,[7] the SMPs have gained a crucial role in fulfilling the increasing demand of materials suitable for smart applications.

The movement associated with the SME made them extensively used for the fabrication of actuators, which are mechanical devices able to change their shape depending on environmental conditions.[8] An external heating source is usually used to stimulate the material response, triggered by the thermal phase transition of the polymeric network.[9–13] In the last few years, several studies have been conducted on shape-memory composites taking advantage of alternative actuation

mechanisms such as chemo-responsive,[14,15] light activated,[16] electro-responsive,[17] and microwave heated SMPs composites.

In particular, the growing demand to get rid of external heating source and the increased interest in self-standing actuators has channeled research efforts towards electro-responsive composites. In this respect, electro-responsive composites have been developed combining thermo-responsive SMPs with an electrically conductive component. External heating is replaced by a DC voltage applied to the material, which is able to activate the SME thanks to the heat dissipation produced by Joule effect.[18,19] An electrically conductive component is necessary owing to the poor electrical conductivity of polymers. However, the presence of such component should provide adequate electrical conductivity without undermining shape-memory properties. One way to obtain a conductive sample is a dispersion of discrete conductive fillers (i.e., CNTs, graphene-oxide, or metallic particles). In this case, the actuation capability of the composite strongly depends on the formation of a percolating conductive network and the homogeneous filler dispersion, making it hard to achieve high-speed actuation. For example, Liu et al. reported a non-uniform temperature distribution during the recovery process caused by an inhomogeneous dispersion of fillers, leading to differences in resistivity along the PU/TiO$_2$ composite.[20]

Furthermore, the high amount of filler needed to obtain enough high electrical conductivity is usually accompanied by high processing viscosities, which may prevent the efficient transfer of properties from filler to matrix.[17]

On the other hand, Luo et al. achieved a significantly high recovery speed using a pre-defined network of non-woven carbon nanofibers (CNFs) incorporated into an epoxy-amine matrix. The highly interconnected CNFs network guaranteed high electrical conductivity and heat transfer efficiency resulting in recovery times within 2 and 18 s.[17] Other excellent papers dealing with electro-active shape memory polymers by adding CNTs are reported by the research group of Prolongo et al., obtaining recovery efficiencies of around 60%–85% triggered at medium voltage (<80 V).[21]

Another successful strategy is to employ conductive layers coated onto SMP surface: Lu et al. developed electrically conductive composites by coating the surface of an epoxy-based SMP with a self-assembled CNFs and boron nitride (BN) nanopaper.[22] The use of BN significantly enhances the thermal coupling of the layers, leading to a recovery speed increase. However, the mismatch of electrical and thermal properties at the bonding interface produced interface dislocations leading to incomplete recovery and low-speed recovery. Considerable enhancement in recovery speed was obtained coupling the epoxy-based SMP with layers of self-assembled carboxylic acid-functionalized CNTs and Nafion/silica nanofiber.[23]

The dual-curing procedure is a valuable tool for preparing shape-memory thermosets and complex shaped actuators. In particular, we demonstrated that thiol-acrylate-epoxy thermosets with relatively low T_g and high quality SME could be obtained via dual curing.[24,25] Our research group also used a dual-curing process to develop a self-standing thermally triggered actuator incorporating a pre-programmed liquid-crystal elastomer layer (LCE, shape-shifting component)

between two layers of glassy thermoset (GT, stress applying component) based on off-stoichiometric thiol-epoxy chemistry.[26,27] The LCE and GT layers were successfully assembled thanks to the dual-curing processing, leading to a very strong adhesion after the second curing stage, as reported by Belmonte et al.[27] Similarly, dual-curing processing could be exploited to incorporate a conductive/heating layer sandwiched between two SMP layers, producing a compact and mechanically consistent piece. The resulting electro-responsive actuator can be programmed in a temporary shape, and the Joule heating produced in the conductive layer can trigger the thermal-activated recovery when needed. The optimal adhesion between layers achieved would produce, in consequence, a compact and durable multi-layered structure with efficient heat transfer between layers and, therefore, efficient actuation upon electrical activation.

In this work, we studied a novel electro-responsive actuation mechanism based on a flexible heater placed between two layers of a recently developed shape-memory thermoset.[25] The heater component consists of a metallic track printed on a thin Kapton® substrate, which has been already employed as a substrate material to fabricate flexible chemo-resistive gas sensors.[28] Two main reasons can be found behind this choice: (i) the combination of Kapton® and the conductive layer would reach a thickness lower than 0.1 mm, so the global stiffness of the SMP actuator should not be significantly affected; (ii) since the heater component is originally designed for wearable sensors, its electrical resistance remains almost constant even during cyclic bending tests.[29] A dual-curing thiol-acrylate-epoxy thermoset[24] was used as SMP, using a suitable ratio between acrylate and thiol groups (r_a) to obtain gelled material after the first curing stage. To enhance the thermal conductivity of the thermosets and therefore enable rapid heating throughout the material, BN particles were dispersed in the thermoset matrix. The electrical activation of the SME was tested using a thermoelectric controlling apparatus enabling the pulse width modulation (PWM) of the electrical current and, consequently, the control of the heating rate. Therefore, the variation of the actuation speed was investigated by varying the average current applied instead of the voltage as commonly found in the literature. This allows us to increase/decrease the actuation speed, always maintaining a low voltage value of 5 V. A comprehensive comparison between the traditional thermal-activated shape recovery experiments and electrically activated shape recovery was also carried out. The effects of multiple parameters, such as BN%, SMP layer thickness, and heating strategies, were evaluated to point out the beneficial effects of the electrical activation compared to the traditional one.

2 | EXPERIMENTAL SECTION

2.1 | Materials

2.1.1 | SMP layer

Thermoset based on a thiol-acrylate-epoxy sequential dual-curing system were used as SMP component. The acrylate monomers employed

are a 50:50 (%wt) mixture of tricyclo[5.2.1.02,6]decanedimethanol diacrylate (TCDDA, Sigma-Aldrich, 152.2 g/eq) and bisphenol A glycero-late (1 glycerol/phenol) diacrylate (BAGA, Sigma-Aldrich, 242.3 g/eq). A commercial epoxy resin, diglycidyl ether of bisphenol A (DGEBA, EPIKOTE™ Resin 828, Hexion specialty chemicals) with an epoxy equivalent weight of 187 g/eq was used as the main epoxy resin. In addition, a tri(2,3-epoxypropyl)isocyanurate (ISO, Sigma-Aldrich) with an epoxy equivalent weight of 99.09 g/eq was used as modifier. The proportion between BAGA and DGEBA is fixed at 50:50 (%wt). Pentaerythritol tetrakis(3-mercapto-propionate) (S4, Sigma-Aldrich), with a molecular weight per thiol equivalent unit of 122.17 g/e, was used as thiol crosslinker maintaining the ratio between acrylate and thiol groups fixed at 0.5 (r_a = 0.5). 4-(N,N-dimethylamino)pyridine (DMAP, Fluka) was used as catalyst for both reactions. 0.05 phr of DMAP were used in all formulations. BN-loaded thermoset layers containing 10 and 15%wt of BN agglomerate (80 μm average, PCTL5MHF, supplied by Saint-Gobain), were prepared by adding BN to the previous formulations.

2.1.2 | Conductive heater

The conductive heater is shown in Figure 1A. The electrode and heater patterns are made of a DuPont® 5064H silver ink (DuPont Inc.) with a solid content between 63 and 66%, a viscosity of 10–20 Pa s and a resistivity ≤6 mΩ/sq/25 μm. The polymer substrate is a 50 μm Kapton® film supplied by DuPont Inc.. Substrate material and silver ink specifics are summarized in Table 1. Firstly, substrates were cleaned in an acetone bath for 5 min, followed by an ethanol bath for 5 min and, at last, rinsed with deionized water and dried at 110°C for 10 min. Once substrates were cleaned, the stencil technique used in our previous research[28] was employed to deposit the electrode and heater onto the substrate. The heater pattern showed in Figure 1B was designed to meet four major requirements: (i) low energy consumption; (ii) rapid activation intended as a short time needed to reach the required activation temperature; (iii) homogeneous temperature distribution throughout the sample surface and (iv) a design easy to print. As shown in Figure 1C, different heating profiles can be obtained controlling the current passing through the heater: increasing the current the target temperature can be achieved in a shorter time.

2.1.3 | Preparation of thermo-responsive SMPs

Neat samples were prepared following the procedure described in our previous work[25] and using suitable molds and a curing schedule consisting of a first curing stage of 2 h at 40°C followed by a second curing stage of 4 h at 80°C. Loaded samples were prepared by adding 10 and 15 wt% of BN agglomerate to the formulation. The formulations were mechanically stirred until a homogeneous mixture was obtained and cured following the same curing schedule of the neat sample. From this point on, SMPs thus obtained, when thermally activated, will be named thermo-responsive actuators (TRA).
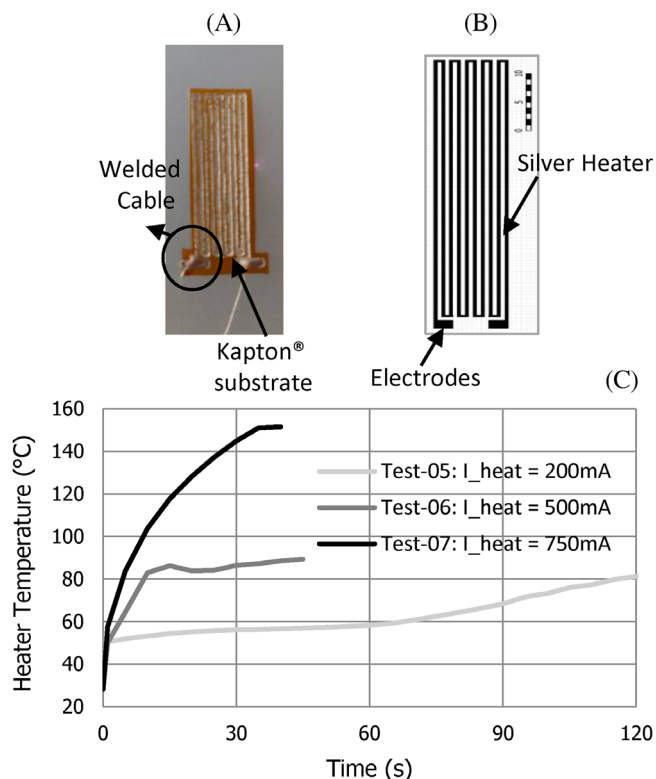

FIGURE 1 (A) Actual photograph of the conductive layer. (B) Schematic representation of the printed silver net. (C) Preliminary measurements performed with a thiol-epoxy thermoset film of 0.4 mm used for testing purpose: heating profiles obtained varying the heating current

TABLE 1 Kapton® HPP-ST and Silver ink 5064H specifics

	Kapton®	Silver ink
Resistivity at 20°C (Ω m)	1.5×10^{15}	1.6×10^{-8}
Thermal linear expansion coefficient (K^{-1})	0.00002	0.002209
Thermal conductivity (W m^{-1} K^{-1})	0.12	429
Density (kg m^{-3})	1420	10,490
Heat capacity (J kg^{-1} K)	1090	232

2.1.4 | Preparation of the electro-responsive actuator

First, intermediate cured SMP material sheets were obtained after the first curing stage of 2 h at 40°C. Large sheets of 30 × 30 mm² with three different thicknesses of 0.4, 0.8, and 1.4 mm were prepared. The heater (9 × 23 mm²) is placed on a SMP sheet (Figure 2A), and a second SMP layer with the same thickness is placed on top in order to obtain the sandwich design (Figure 2B). The SMP excess is cut away from the sandwich, leaving an exceeding width of 1 mm on both sides (Figure 2B). The actuator was designed with an excess of SMP on

both edges in order to ensure good contact between the two layers of SMP and, consequently, to achieve a perfect fit of the conductive component within the SMP. The assembly is then confined using Teflon spacers and lightly fastened between Teflon-coated glass plates (Figure 2C). Finally, the second curing stage of the SMP material is performed (4 h at 80°C), leading to the desired actuator configuration. The multi-layered actuators obtained, activated by the electrical stimulus, will be named electro-responsive actuators (ERA).

2.2 | Thermoelectric control apparatus (controlling unit)

The thermoelectric control of the actuator is conducted by an electronic board equipped with a microcontroller, a load switch, a current sensor and a temperature sensor. The microcontroller commands the load switch by pulse-width modulation (PWM), allowing the regulation of the average current supplied to the heater (Figure 3). The

microcontroller also drives the heater switch off when the actuator reaches the required temperature.

PWM is a digital modulation commonly used to control "slow" physical processes. The control signal periodically switches on and off at a relative "high" frequency, delivering power to the system in a digitally discontinuous mode. However, as long as the system time constant is sufficiently higher than the switching period, it will be perceived as an average continuous amount of energy, thereby enabling the direct control of systems with high inertias without using added electronics to perform the low pass filtering of the digitally modulated signal. This is the usual way of controlling electric motors speed or LED lamps glowing intensity. In our case, the heat released per time unit will be related to the t_{on}/t_{PWM} ratio (duty cycle), where t_{on} is the time the signal is "on", and t_{PWM} is the PWM signal period. In this way, we can control how quickly the temperature increases just varying this duty cycle (the higher the t_{on}, the faster the temperature increase is obtained).

Additionally, the temperature of the heater (T_{Heat}) can be indirectly measured at any time. Taking advantage of the quasi-linear
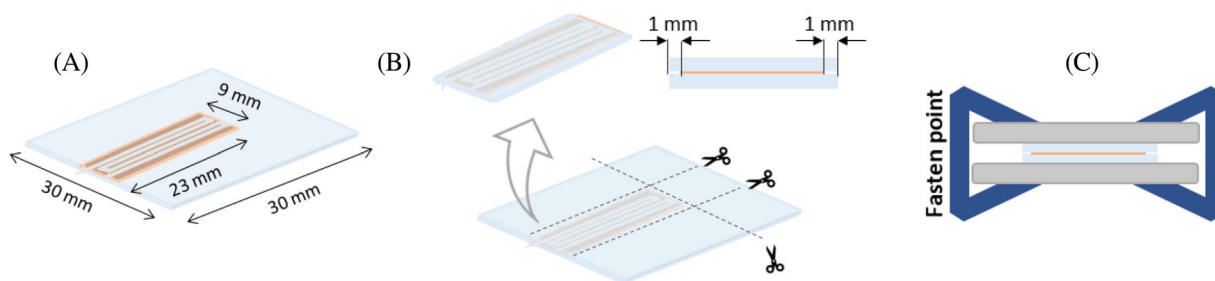

FIGURE 2 Schematic representation of the electro-responsive actuator (ERA) assembling: (A) assembling of the first shape-memory polymer (SMP) layer and the heater; (B) assembling of the second SMP layer and cutting to final dimensions; (C) Second curing stage of the assembled actuator
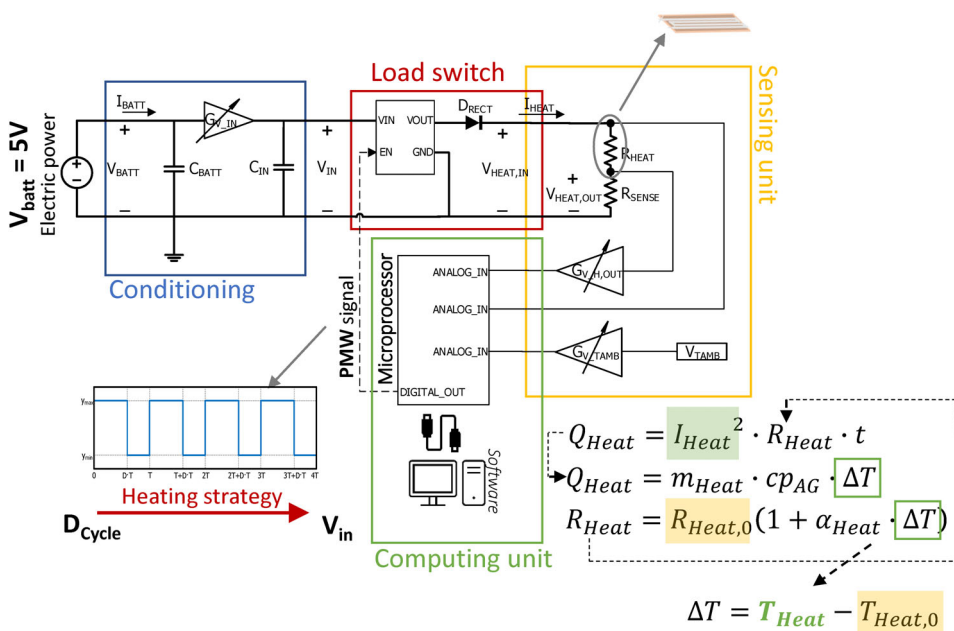

$$Q_{Heat} = I_{Heat}^2 \cdot R_{Heat} \cdot t$$

$$Q_{Heat} = m_{Heat} \cdot cp_{AG} \cdot \Delta T$$

$$R_{Heat} = R_{Heat,0}(1 + \alpha_{Heat} \cdot \Delta T)$$

$$\Delta T = T_{Heat} - T_{Heat,0}$$

FIGURE 3 Schematic representation of the thermoelectric control of the actuation

behavior of the metallic resistances at varying temperatures, the resistance of the heater (R_{Heat}) can be computed as:

$$R_{Heat} = R_{Heat,0} \cdot (1 + \alpha_{Heat} \times (T_{Heat} - T_{Heat,0})), \tag{1}$$

where $R_{Heat,0}$ is the initial value of the heater resistance, α_{Heat} is the thermal conductivity of the heater and $T_{Heat,0}$ is the initial temperature of the heater. Using an ambient temperature sensor together with the $V_{Heat,in}$ (the input voltage of the heater) sensing, $T_{Heat,0}$ and $R_{Heat,0}$ can be easily measured at the beginning of every experiment. In order to measure R_{Heat}, a shunt resistance $R_{sens} = 10$ mΩ (precisely calibrated and with a very low value that is not heated and remains constant) was added. The value of R_{Heat} can be deduced from the circuit analysis (the sensing unit is schematically represented in Figure 3) as follows:

$$R_{Heat} = R_{sens} \cdot \left(\frac{V_{Heat,in}}{V_{Heat,out}} - 1 \right), \tag{2}$$

where the heater output voltage ($V_{Heat,out}$) is measured by the microcontroller as $I_{Heat} \cdot R_{sens}$. In this way, combining Equations (1) and (2), the microcontroller can easily calculate the T_{Heat} during every experiment, for any device, at any room temperature and any supplied voltage (V_{batt}).

The microcontroller also performs some user interface tasks. Once the actuator is connected to the apparatus, the software interface requires the insertion of a set-point temperature (T_{set}), which is the target temperature the actuator should reach, and the heating strategy (related to the time spent in reaching the target temperature). The heating strategies are named after the percentage value of the maximum speed at which the set-point temperature is reached. In this paper, the electro-responsive actuators (ERAs) were heated at $T_{set} = 120°C$ employing three heating strategies (25%, 50%, and 100% heating speed). At the same time, the power supply was limited at $V_{Batt} = 5$ V. Using this controlling board, many different actuation strategies can be studied by modulating the heating current, maintaining the supply voltage constant, and with a very low value (in the working range of a USB charger).

2.3 | Characterization of the TRAs

Dynamic mechanical analysis was performed to characterize the effect of BN% on the thermomechanical properties of the SMP in use. TA Instruments dynamic mechanical analyzer (DMA) Q800 equipped with a three-point bending clamp (15 mm) was used to characterize the relaxation process. Prismatic rectangular samples ($15 \times 6 \times 2.5$ mm^3) were analyzed in oscillation mode at 1 Hz, 0.1% of strain amplitude and at a heating rate of 3°C/min from 20 to 150°C. The T_g was determined as the tanδ peak temperature, and glassy (E_g) and rubbery (E_r) moduli were determined at 0 and 100°C, respectively.

The flexural modulus (E_{SMP}) of final SMPs was determined with the same apparatus and clamp with a force ramp at a constant rate of 1 N/min in controlled force mode. The slope (m) within the linear zone of the force-displacement curve was obtained, and E_{SMP} was calculated following Equation (3):

$$E_{SMP} = \frac{L^3 m}{4wt^3} \tag{3}$$

where L is the support span, and w and t are the width and thickness of the test sample, respectively.

The thermal conductivity of the SMP was measured using the Transient Hot Bridge method (THB) using a THB 100 device from Linseis Messgeräte GmbH. An HTP G 9161 sensor was used with a 3×3 mm^2 area calibrated with polymethylmethacrylate (PMMA), borosilicate crown glass, marble, Ti–Al alloy, and titanium. Two equal polished circular SMP samples (10 mm in diameter and 2.3 mm in thickness) were placed in each face of the sensor. Due to the small size of the sensor, side effects can be neglected. A measuring time of 100 s with a current of 10 mA was applied to the five measures done for each different formulation.

The thermally activated shape recovery of all the TRAs was recorded through free recovery experiments carried out using the DMA equipment in force-controlled mode, equipped with a 3-point bending clamp (15 mm). Rectangular flat samples ($11 \times 25 \times 0.8$ mm^3) were previously programmed in a curved shape following the next steps: (i) the sample was heated up in an oven to the programming temperature ($T_g + 20°C$), and then deformed to a curved shape using a bending guide a shown in Figure 4A; (ii) the bending guide and the sample were rapidly cooled down with ice water while maintaining the force applied; (iii) finally samples were unloaded. The programmed (curved) samples were placed on the DMA clamp as shown in Figure 4B left, and the shape-recovery process was monitored under constant heating rates of 3, 5, and 10°C/min until the final shape (flat) is recovered (Figure 4B right). A slight preload force of 0.1 N was used to ensure good contact with the sample during the monitoring of the shape recovery process. Figure 4C shows a schematic representation of the experimental setup. The displacement of the movable clamp $d(T)$ was used to calculate the shape recovery rate, SR(%), following Equation (4):

$$SR(\%) = \left(1 - \frac{d(t)}{d_{max}} \right) \times 100, \tag{4}$$

where d_{max} is the displacement obtained by the original shape prior to sample programming. The instantaneous shape-recovery speed $SR_{speed}(T)$ was calculated by Equation (5):

$$SR_{speed} = \frac{\partial SR(T)}{\partial T}. \tag{5}$$

Using the $SR_{speed}(T)$ curve, the temperature of maximum recovery speed and the temperature range of the process were determined as the peak of the curve (T_{peak}) and as the width of the curve at half-height (ΔT_{peak}), respectively.
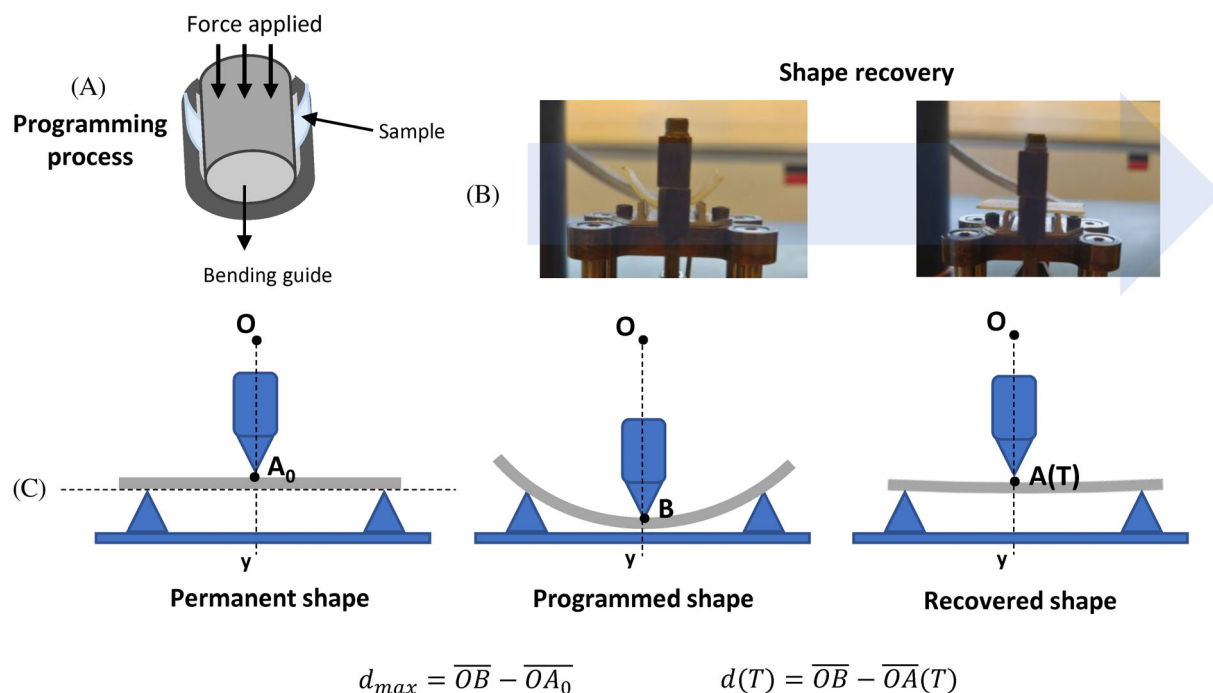
FIGURE 4   DMA unconstrained recovery experiments: (A) programming process; (B) sample leaned on the DMA clamp before and after the recovery process; and (C) illustration of the DMA testing procedure

2.4 | Characterization of the ERAs

The flexural modulus of the electro-responsive actuator (E_{ERA}) was determined by a DMA force-controlled analysis as detailed in the above section. DMA oscillatory analyses on the assembled actuator were also performed to determine the effect of the layered structure on the thermomechanical properties. TA Instruments DMA Q800 equipped with a three-point bending clamp (15 mm) was used. Assembled ERAs were tested at 1 Hz, 0.1% strain amplitude, and 3°C/min heating rate.

The electrically activated shape recovery of the actuator was analyzed as follows. The programming process was performed with the same methodology described in Section 2.3 (Figure 4A). After removing the force applied, the sample was perfectly dried and connected to the controlling unit to activate and monitor the shape recovery. The electro-responsive actuators were heated at $T_{set} = 120\,°C$ employing three heating strategies, 25%, 50%, and 100%, while the power supply is limited at 5 V ($V_{Batt} = 5$ V). The recovery strategies were named fast, medium, and slow, indicating the 100%, 50%, and 25% strategies, respectively. The recovery process was recorded using a high-resolution camera and further analyzed frame by frame, measuring the angles as shown in Figure 5 and applying Equation (6) on each frame.

$$SR(\%) = \frac{\theta_t - \theta_0}{180° - \theta_0} \times 100, \tag{6}$$

where SR(%) is the percentage of shape recovery, θ_0 is the angle at $t = 0$ s and θ_t is the angle at time t. A frame interval of 1 s was used

for 50% and 25% strategies, while a frame interval of 0.25 s was used for 100% strategy.

3 | RESULTS

3.1 | Characterization of the TRAs

Thermomechanical properties of fully cured SMPs were investigated to assess the effect of the BN particles, which are expected to increase the material toughness without altering the T_g.[30] Moreover, BN particles are proven not to increase the electrical conductivity of epoxy-based thermosets, keeping their electrical insulation.[30,31] In Figure 6, the evolution of storage modulus and tanδ with respect to temperature are presented. As expected, incorporating 10%wt BN filler leads to a noticeable increase in the storage modulus, while only a slight increase was found when increasing BN filler content from 10 to 15%wt. On the other hand, it can be observed that the glass transition (peak of the tanδ) is not significantly affected by the filler. DMA results are summarized in Table 2 together with the measured value of E_{SMP}. BN loaded samples showed a similar value of T_g while the FWHM slightly increased, probably due to a slight increase in network heterogeneity. It is noteworthy that only a small broadening of tanδ evolution is present, otherwise, shape-memory properties would have been adversely affected in terms of recovery speed.[32] Furthermore, the increase of BN %wt leads to an enhancement of the rubbery modulus E'_r, which also has beneficial effects on shape-memory properties, particularly in constrained recovery processes. With respect to the flexural moduli measured at 25°C, it increases about

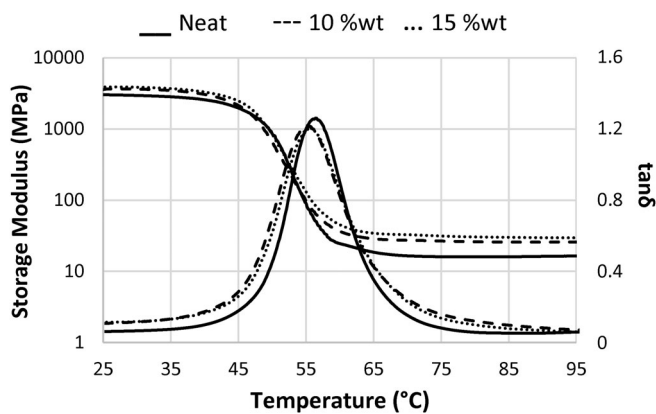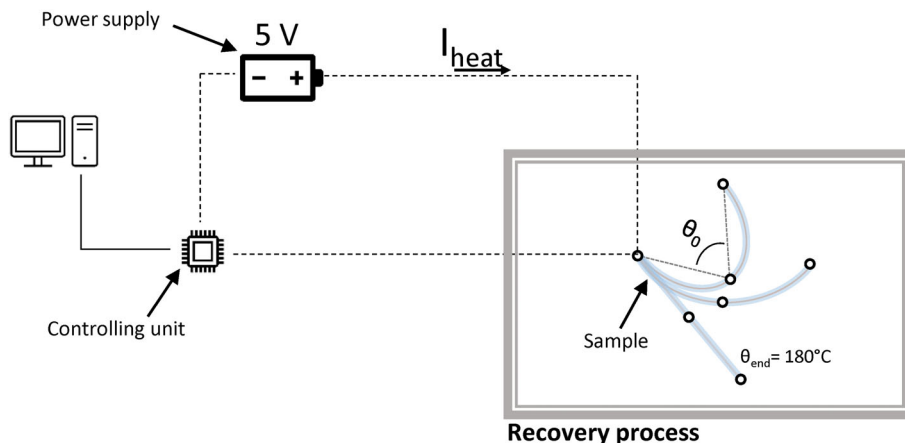**FIGURE 5** Schematic representation of shape-recovery scenario

Recovery process

FIGURE 6 Evolution of storage modulus and tanδ with temperature during DMA analysis on the shape-memory polymers tested

50% when 10%wt of BN is used, and almost a 70% in case of 15%wt of BN, as a direct consequence of the presence of filler.

The effect of increasing %wt of BN on thermal conductivity was also investigated, and results are presented in Figure 7. Incorporating BN fillers significantly enhances the thermal conductivity of these thermosets: 15 wt% sample reaches a thermal conductivity of 0.587 W/mK, which is almost three times higher than the value reached by the neat sample (0.206 W/mK). This high increase in thermal conductivity has been pursued to ensure the ERAs' high recovery performance. It is acknowledged that higher thermal conductivity will positively affect both Joule and conventional heating processes, allowing faster and more homogenous heating throughout the whole sample in any case. However, this effect is more pronounced in electrical heating because the system can increase the power to reach the target temperature faster than in the oven. If the power is increased but the thermal conductivity is low, the sample can be internally overheated and damaged. This is not the case with external heating where it is difficult to overheat and damage the sample.

The shape-memory behavior of these materials was investigated with free-recovery experiments in DMA apparatus, as explained in Section 2.3. Samples were programmed in an oven, and then the recovery process was monitored with the DMA at different heating rates. When analyzing the recovery process at 3°C/min, it can be observed that the presence of BN filler slightly affects the shape recovery (Figure 8). At this heating rate, the presence of BN slightly retards the recovery process compared to the neat sample. The maximum effect was found for the 15%wt sample, which shows a higher T_{peak} (about 1°C higher) and ΔT_{peak}, leading to an increase of $t_{5\%-95\%}$ from 4.05 to 8.01 min (Table 3). The observed delay can be ascribed to the broader tanδ peak obtained for 10% and 15% samples. Moreover, the recovery of 15%wt seems to slow down in the final stages, probably due to the presence of the filler hindering the network elastic response.

The effect of the heating rate on the recovery process was also investigated to explore a way to control the speed at which the actuation is triggered. As expected, the activation of the shape-recovery is significantly anticipated in time because the sample merely takes less time to reach the activation temperature. Therefore, $t_{5\%-95\%}$ (calculated as the amount of time between 5% and 95% of the recovery process, SR(%)) is significantly reduced to about 1.5 min. Although the recovery process is fast, Figure 8A clearly shows that the T_{peak} increases with the heating rate. This effect can be due to either viscoelastic or heat transmission issues: when the sample is rapidly heated, the material does not have the necessary time to relax its network structure, leading to a delay in the recovery of the shape.

On the other hand, samples in the oven are heated by convection which can produce a slight temperature gradient from the surface to the sample core. Increasing the heating rate produces a more significant gradient, shifting the recovery process to a higher temperature. In this scenario, the difference in T_{peak} between Neat and BN loaded samples is slightly reduced and, at 10°C/min, samples with BN slightly anticipate the neat sample recovery. The higher thermal conductivity obtained with BN particles enhances the heat transmission within the

	E'_g (MPa)[a]	E'_r (MPa)[b]	T_g (°C)	$T_g + 30$ (°C)	FWHM (°C)	E_{SMP} (GPa)[c]
Neat	3067	16.3	56	86	10.1	1.30
10%wt	3637	25.7	55	85	11.8	2.00
15%wt	3881	29.6	55	85	11.6	2.18

[a]Calculated at 20°C.
[b]Calculated at 100°C.
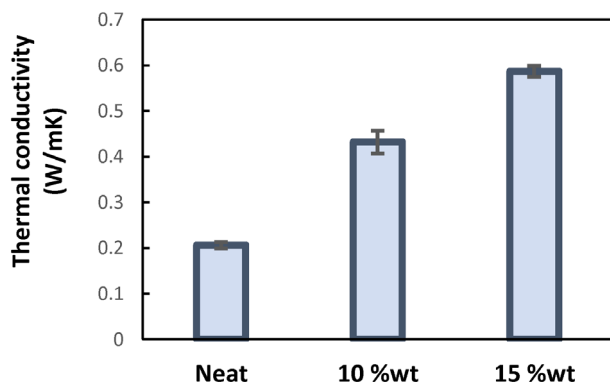[c]Calculated by Equation (3) at 25°C.

FIGURE 7 Thermal conductivity of the shape-memory polymers prepared varying the proportion of boron nitride

sample, reducing the temperature gradient and, therefore, a lower T_{peak}. A clear trend in SR(%) is not visible (Table 3) and all samples recover about 97%–98% at all heating conditions.

3.2 | Electro-responsive actuators characterization

First, thermomechanical properties of the composite assembly were tested together with the resulting flexural modulus. As shown in Figure 9 for the 10%wt BN actuator, the heater positioned at the mid-plane does not significantly affect the thermomechanical behavior. The most visible effect is on the shape of the tanδ peak. As expected, a broader peak is obtained for the actuator due to the heterogeneity of the sample resulting from the assembly of the different layers. Although the SMP layers have identical properties and T_g, the Kapton® substrate of the heating layer has a T_g between 360 and 410°C. Therefore it remains in the glassy state while the other layers relax. Despite so, even in the rubbery region, where the glassy Kapton® response could be dominant, only a slight increase of E'_r is detected. The flexural modulus of the assembled actuator was also measured, and the results are presented in Table 4. It can be seen that the flexural moduli of the assembled samples show only a slight increase with respect to E_{SMP} in all %wt of BN, probably owing to the incorporation of the more rigid layer. In light of these findings, we assume that the presence of the intermediate layer would not results in appreciable effects on the SME.

The recovery process of the electro-responsive actuators was tested in unconstrained conditions under 5 V of applied voltage.

Preprogrammed ERAs were connected to the controlling unit which can modulate the current passing through the heater at three different levels, corresponding to three heating strategies: fast, medium and slow. In order to minimize any eventual external friction, samples were hung midair with a gripper. The shape-recovery process over time is reported in Figure 10. In contrast with classical thermal triggering, the higher thermal conductivity obtained with BN fillers clearly results in faster activation of the recovery process and reduced recovery time (Table 5). In this configuration, the sample got heated up from the inner layer and therefore, thermal conductivity plays a crucial role in accelerating the heat transmission outwards. Loaded samples took less time to recover the initial shape in all three activation conditions.

The best results are obtained by the 15%wt ERA, which could recover almost the 100% of the original shape in just 8 s with the fast heating strategy (Figure 10A). In particular, loaded samples could recover 80% of the original shape in only 4 s; then, the recovery process slightly slowed down, probably due to a network structural effect. Recovery time and velocity can be controlled by the intensity of the current responsible for the Joule heating. Gradually slower recovery processes are obtained by reducing the heating current, as shown in Figures 10B,C. The highest recovery ratios between 99% and 100% are obtained with fast and medium strategies, while slightly lower recovery ratios (around 97%) are obtained with the slow heating strategy. This effect can be ascribed to a less powerful Joule heating originated by the lower current intensity employed for the slow strategy.

In order to better understand the electro-activated shape-recovery process, the time-dependent temperature profiles of 10 wt% of BN loaded ERA were determined for all heating strategies (Figure 10D). Heating profiles were obtained using a PT100 temperature probe stuck on the SMP surface during heating. As expected, the heating rate strongly increases with the I_{heat} (from slow to fast strategy), as well as the maximum temperature reached on the surface of the ERA also increases. Although the $T_{set} = 120$°C was only reached with the fast strategy, all strategies can easily reach the actuation temperature. In particular, the ERA recovers the initial shape in the same temperature range for all heating strategies and at a temperature close to the T_{peak} found for 3°C/min recovery experiment in DMA.

The possibility of controlling the recovery process speed can be exploited to obtain different actuation strategies that can be adjusted to the final application. In bending mode, for constrained recovery or partially constrained process, the thickness of the actuator is a
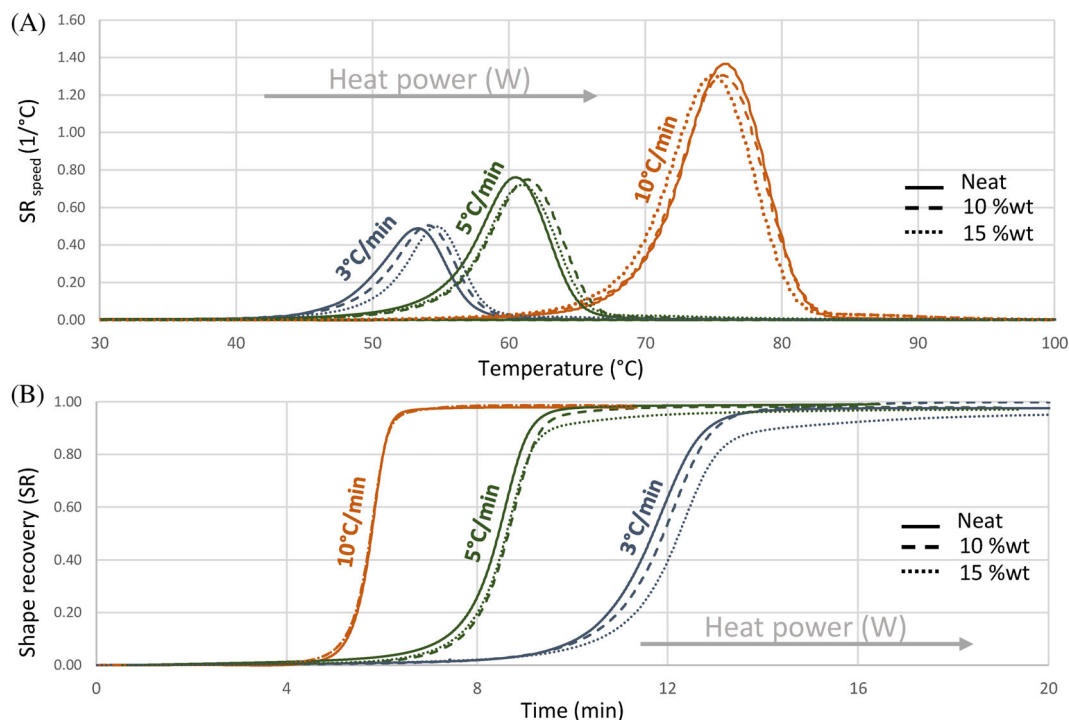
FIGURE 8 Free recovery experiments at three different heating rates: (A) instantaneous recovery speed evolution with temperature; and (B) Shape-recovery evolution along time

TABLE 3 Parameters obtained from unconstrained shape-memory analysis at different heating rates. Coefficients of variation less than 2%

	BN %wt	T_{peak} (°C)	ΔT_{peak} (°C)	SR (%)	$t_{5\%-95\%}$ (min)
3°C/min	0	53.4	5.1	97.7	4.05
	10	54.6	5.2	99.7	4.08
	15	54.9	5.4	97.3	8.01
5°C/min	0	60.5	5.9	99.1	2.85
	10	61.4	5.9	98.6	2.77
	15	61.0	6.4	97.5	4.89
10°C/min	0	75.9	6.9	98.0	1.30
	10	75.7	7.0	98.7	1.50
	15	74.8	7.1	98.1	1.48

commanding parameter because higher recovery forces or higher work output can be obtained with higher thicknesses. Therefore, the effect of increasing the t_{layer} of SMP with 10 wt% of BN was also tested with all heating strategies and the results are shown in Figure 11. In Figure 11, the induction time is defined as the time needed to reach a SR(%) = 3%. Thicker layers produce the increase of the total recovery time and a significant increase of the induction time or the time the sample takes to get heated from ambient temperature to the start of the transition process. The more significant effect can be seen for the slow heating strategy (25%). As discussed above, the lower current intensity produces a less powerful Joule heating which, combined with the higher layer thickness, results in

a significant induction time between 20 and 40 s, depending on the thickness.

Regarding the results obtained when heating in the oven, the electrically activated shape-recovery is enormously fast and efficient, even with thicker SMP layers: moderate energy level is employed to heat the material with almost no energy losses. On the other hand, for traditional thermally activated actuation, extra heat power is always required to increase the whole ambient temperature, wasting much more energy than the actual heat needed by the sample.[33]

From the above-presented results, it can be seen that high-speed actuation at relatively low voltage has been obtained. The combined
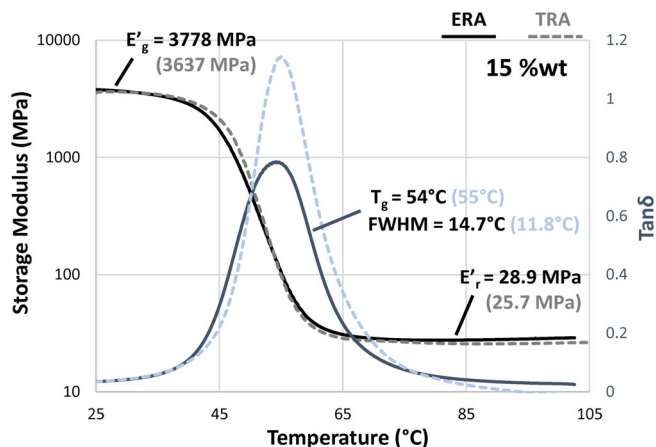
FIGURE 9 DMA analysis of 10%wt boron nitride (BN) (BN) electro-responsive actuators (both shape-memory polymer layers thickness are 0.4 mm each) compared with the 10%wt BN thermo-responsive actuators (TRA) (0.8 mm thickness): characteristic thermomechanical data are also indicated (values obtained for the 10%wt BN TRA in brackets)

TABLE 4 Flexural modulus values of the electro-responsive actuators (ERAs) and thermo-responsive actuators (TRAs) samples. Coefficients of variation less than 5%

BN (%wt)	E_{SMP} (GPa)[a]	$E_{Kapton®}$ (GPa)[b]	E_{ERA} (GPa)[c]
0	1.30	2.8	1.38
10	2.00		2.10
15	2.18		2.34

[a]0.8 mm thickness.
[b]Tensile modulus.
[c]0.4 mm SMP layers thickness.

use of BN particles and conductive heater layer leads to recovery times lower than other electro-responsive actuators found in literature: PU-TiO$_2$ SMP composites developed by Liu et al. recovered their permanent shape in about 60 s under 70 V applied[20]; epoxy-based SMP composites presented by Lu et al. achieved complete recovery in 74 s (4.8 V)[22]; PU composites incorporating printed carbon nanotube layers proposed by Wang et al. recover the shape in about 30 s.[34] Bilayer shape-memory composites developed by Zheng et al.[35] took around 220 s to recover their shape under 5 V voltage applied. Higher actuation speed can be found in the literature but at significantly higher voltage (around 20–40 V).[17,21,36,37] The comparison in terms of power (W) is not always possible due to insufficient data available. In this investigation, electro-activated SM experiments were conducted applying 0.84, 1.8, and 3.5 W (respectively slow, medium and fast) depending on the heating strategies. Similar electric power values were found for RGOP/epoxy composites,[36] which recovered the shape in 5 s when 3.6 W were applied. Lu et al.[22] shape-memory nanocomposites recovered the initial shape in 72 s when 2.3 W were applied, while, with the medium heating strategy (1.8 W), our actuator showed a significantly faster recovery. Recently, electroactive polymer composites for soft actuators developed by An et al.[38] reached similar recovery times (7 s) with lower electric power (less than 1 W) applied.

As it can be concluded, the voltage supplied to our thermoelectric control is the USB standard voltage, and the value of current is well below the maximum value provided by a commercial USB charger. The flexibility in terms of power source is a strong point in favor of the applicability of our system.
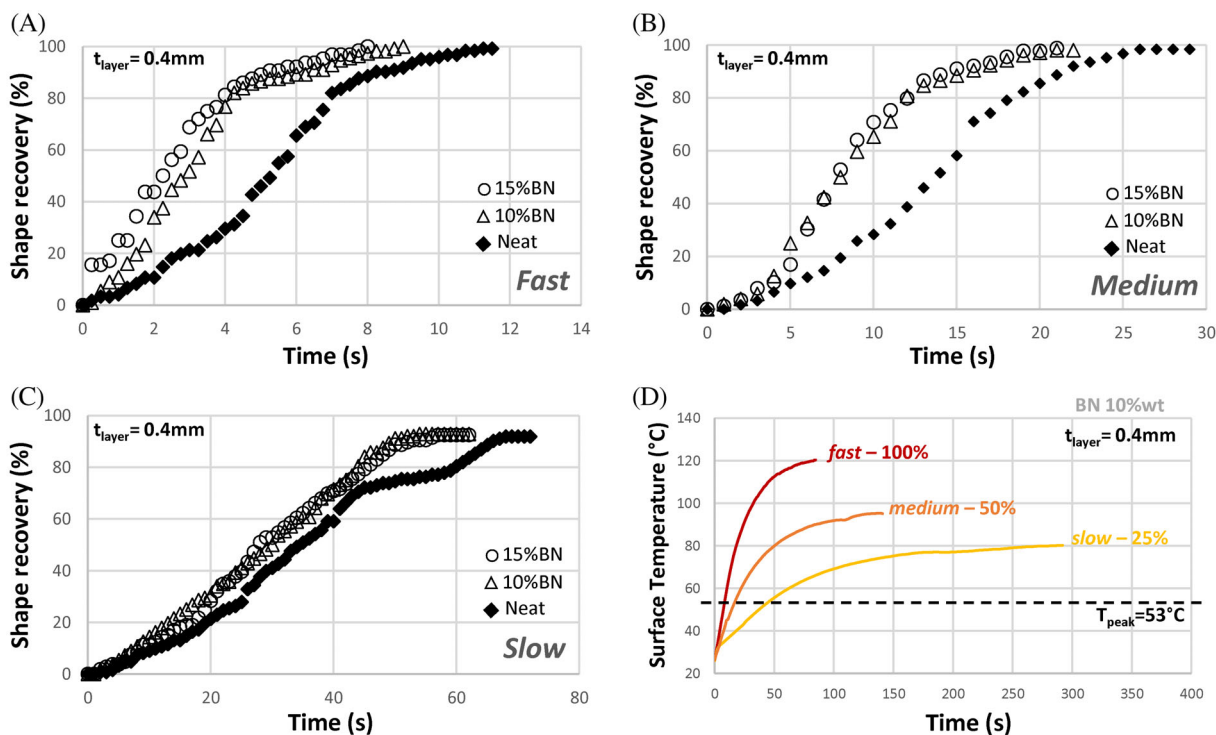

FIGURE 10 (A) Shape recovery ratio over time for the fast heating strategy. (B) Shape recovery ratio over time for the medium heating strategy. (C) Shape recovery ratio over time for the slow heating strategy. (D) Joule heating profiles of electro-responsive actuators loaded with 10%wt of boron nitride

TABLE 5 Characteristic values of the electrically triggered recovery process at three different actuation strategies. Coefficients of variation less than 2% for shape-recovery data

	t_{layer} (mm)[a]	Fast—701 mA		Medium—361 mA		Slow—168 mA	
		$t_{recovey}$ (s)	$v_{recovery}$ (%/s)	$t_{recovey}$ (s)	$v_{recovery}$ (%/s)	$t_{recovey}$ (s)	$v_{recovery}$ (%/s)
Neat	0.4	11.2	15.9	26.0	6.1	68.0	1.6
10%wt	0.4	9.0	19.8	21.0	7.9	58.0	1.9
15%wt	0.4	8.0	22.3	21.0	9.1	57.0	2.0

[a]t_{layer} is the thickness of each of both shape-memory polymer layers.
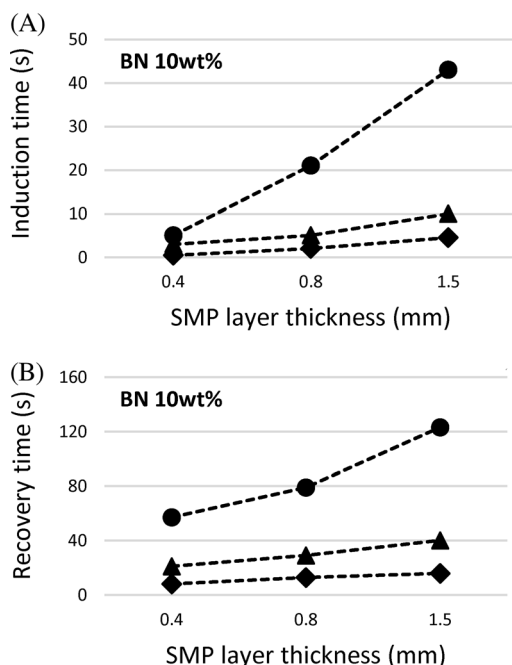
FIGURE 11 Variation of the induction time (A) and recovery time (B) with shape-memory polymer thickness at three actuation strategies: slow (●), medium (▲), and fast (◆)

4 | CONCLUSIONS

Novel electro-responsive shape-memory actuators were developed combining dual-cured SMPs and flexible conductive heaters. The dual-curing processing was exploited to incorporate the conductive heater in the SMP. First, 10 and 15% of BN agglomerates were added to the SMP matrix to increase thermal conductivity. The addition of BN fillers led to a 300% increase of thermal conductivity and an increase of flexural modulus around 70%, while the relaxation process is not significantly affected. A thermoelectric controlling unit was designed in order to characterize the electrical activation of the SME. The shape-memory behavior of the thermo-responsive and the electro-responsive actuator was characterized and compared to determine the advantages of the electrically driven Joule heating in front of the traditional external heating. The SME was tested at different heating rates or heating strategies in both activation mechanisms. The electro-responsive actuators demonstrated significantly higher

recovery velocity than traditional thermo-responsive actuators; the lowest recovery time achieved was the 8 s reached by the 15% BN actuator with the fast heating strategy. The effect of the increased thermal conductivity was also visible since the increase of BN% led to faster recovery with all heating strategies. Finally, the controlling unit proposed in this work allowed an excellent control on the recovery process by providing a different heating strategy maintaining a fixed and low value of voltage (5 V).

CONFLICT OF INTEREST

The authors declare that they have no known competing financial interests or personal relationships that could have appeared to influence the work reported in this paper.

DATA AVAILABILITY STATEMENT

The datasets generated during and/or analysed during the current study are available from the corresponding author on reasonable request.

ORCID

Silvia De la Flor https://orcid.org/0000-0002-6851-1371

REFERENCES

1. Safranski DL. *Introduction to Shape-Memory Polymers*. Elsevier Inc; 2017.
2. Lendlein A, Kelch S. Shape-memory effect. *Angew Chem Int Ed*. 2002; 41:2034-2037. doi:10.1002/1521-3773(20020617)41:12%3C2034:: AID-ANIE2034%3E3.0.CO;2-M
3. Balk M, Behl M, Wischke C, Zotzmann J, Lendlein A. Recent advances in degradable lactide-based shape-memory polymers. *Adv Drug Deliv Rev*. 2016;107:136-152. doi:10.1016/j.addr.2016.05.012
4. Yakacki CM, Shandas R, Lanning C, Rech B, Eckstein A, Gall K. Unconstrained recovery characterization of shape-memory polymer networks for cardiovascular applications. *Biomaterials*. 2007;28:2255-2263. doi:10.1016/j.biomaterials.2007.01.030
5. Maitland DJ, Metzger MF, Schumann D, Lee A, Wilson TS. Photothermal properties of shape memory polymer micro-actuators for treating stroke. *Lasers Surg Med*. 2002;30:1-11. doi:10.1002/lsm.10007

6. Sun J, Guan Q, Liu Y, Leng J. Morphing aircraft based on smart materials and structures: a state-of-the-art review. *J Intell Mater Syst Struct*. 2016;27:2289-2312. doi:10.1177/1045389X16629569

7. Tobushi H, Hayashi S, Hoshio K, Ejiri Y. Shape recovery and irrecoverable strain control in polyurethane shape-memory polymer. *Sci Technol Adv Mater*. 2008;9:015009. doi:10.1088/1468-6996/9/1/015009

8. Gopinath S, Mathew S, Nair PR. Shape memory actuators. In: Boddula R, Inamuddin, Asiri AM, eds. *Actuators: Fundamentals, Principles, Materials and Applications*. New York, NY: Wiley; 2020;139-158.

9. Lendlein A, Sauter T. Shape-memory effect in polymers. *Macromol Chem Phys*. 2013;214:1175-1177. doi:10.1002/macp.201300098

10. Heuchel M, Sauter T, Kratz K, Lendlein A. Thermally induced shape-memory effects in polymers: quantification and related modeling approaches. *J Polym Sci Part B: Polym Phys*. 2013;51:621-637. doi:10.1002/polb.23251

11. Yakacki CM, Shandas R, Safranski D, Ortega AM, Sassaman K, Gall K. Strong, tailored, biocompatible shape-memory polymer networks. *Adv Funct Mater*. 2008;18:2428-2435. doi:10.1002/adfm.200701049

12. Nair DP, Cramer NB, Scott TF, Bowman CN, Shandas R. Photopolymerized thiol-ene systems as shape memory polymers. *Polymer*. 2010;51:4383-4389. doi:10.1016/j.polymer.2010.07.027

13. Belmonte A, Russo C, Ambrogi V, Fernández-Francos X, la Flor SD. Epoxy-based shape-memory actuators obtained via dual-curing of off-stoichiometric "thiol-epoxy" mixtures. *Polymers*. 2017;9(3):1-19. doi:10.3390/polym9030113

14. Correia CO, Leite ÁJ, Mano JF. Chitosan/bioactive glass nanoparticles scaffolds with shape memory properties. *Carbohydr Polym*. 2015;123:39-45. doi:10.1016/j.carbpol.2014.12.076

15. Boyle AJ, Weems AC, Hasan SM, Nash LD, Monroe MBB, Maitland DJ. Solvent stimulated actuation of polyurethane-based shape memory polymer foams using dimethyl sulfoxide and ethanol. *Smart Mater Struct*. 2016;25:075014. doi:10.1088/0964-1726/25/7/075014

16. Yang H, Leow WR, Wang T, et al. 3D printed photoresponsive devices based on shape memory composites. *Adv Mater*. 2017;29:1701627. doi:10.1002/adma.201701627

17. Luo X, Mather PT. Conductive shape memory nanocomposites for high speed electrical actuation. *Soft Matter*. 2010;6:2146-2149. doi:10.1039/C001295E

18. Slobodian P, Riha P, Olejnik R, Matyas J. Accelerated shape forming and recovering, induction, and release of adhesiveness of conductive carbon nanotube/epoxy composites by joule heating. *Polymers*. 2020;12:1030. doi:10.3390/polym12051030

19. Sánchez-Romate XF, Sans A, Jiménez-Suárez A, Campo M, Ureña A, Prolongo SG. Highly multifunctional GNP/epoxy nanocomposites: from strain-sensing to joule heating applications. *Nanomaterials*. 2020;10:2431. doi:10.3390/nano10122431

20. Liu W, Chen H, Ge M, Ni QQ, Gao Q. Electroactive shape memory composites with TiO₂ whiskers for switching an electrical circuit. *Mater Des*. 2018;143:196-203. doi:10.1016/j.matdes.2018.02.005

21. Prolongo SG, Díaz-Maroto CG, Jiménez-Suárez A. Electroactive shaping and shape memory of sequential dual-cured off-stoichiometric epoxy/CNT composites. *J Mater Res Technol*. 2021;15:2970-2981. doi:10.1016/j.jmrt.2021.09.102

22. Lu H, Huang WM, Leng J. Functionally graded and self-assembled carbon nanofiber and boron nitride in nanopaper for electrical actuation of shape memory nanocomposites. *Compos Part B: Eng*. 2014;62:1-4. doi:10.1016/j.compositesb.2014.02.003

23. Lu H, Yin J, Xu B, Gou J, Hui D, Fu Y. Synergistic effects of carboxylic acid-functionalized carbon nanotube and nafion/silica nanofiber on electrical actuation efficiency of shape memory polymer nanocomposite. *Compos Part B: Eng*. 2016;100:146-151. doi:10.1016/j.compositesb.2016.06.072

24. Russo C, Serra À, Fernández-Francos X, la Flor SD. Characterization of sequential dual-curing of thiol-acrylate-epoxy systems with controlled thermal properties. *Eur Polym J*. 2019;112:376-388. doi:10.1016/j.eurpolymj.2018.12.048

25. Russo C, Fernandez-Francos X, De la Flor S. Shape-memory actuators based on dual-curing thiol-acrylate-epoxy thermosets. *Express Polym Lett*. 2021;15:58-71. doi:10.3144/expresspolymlett.2021.7

26. Belmonte A, Lama GC, Cerruti P, Ambrogi V, Fernández-Francos X, De la Flor S. Motion control in free-standing shape-memory actuators. *Smart Mater Struct*. 2018;27:075013. doi:10.1088/1361-665X/aac278

27. Belmonte A, Lama GC, Gentile G, et al. Thermally-triggered free-standing shape-memory actuators. *Eur Polym J*. 2017;97:241-252. doi:10.1016/j.eurpolymj.2017.10.006

28. Alvarado M, Navarrete È, Romero A, Ramírez JL, Llobet E. Flexible gas sensors employing octahedral indium oxide films. *Sensors*. 2018;18:999. doi:10.3390/s18040999

29. Alvarado M, la Flor SD, Llobet E, Romero A, Ramírez JL. Performance of flexible chemoresistive gas sensors after having undergone automated bending tests. *Sensors*. 2019;19:5190. doi:10.3390/s19235190

30. Isarn I, Gamardella F, Massagués L, Fernández-Francos X, Serra À, Ferrando F. New epoxy composite thermosets with enhanced thermal conductivity and high Tg obtained by cationic homopolymerization. *Polym Compos*. 2018;39:760-769. doi:10.1002/pc.24774

31. Isarn I, Bonnaud L, Massagués L, Serra À, Ferrando F. Enhancement of thermal conductivity in epoxy coatings through the combined addition of expanded graphite and boron nitride fillers. *Prog Org Coat*. 2019;133:299-308. doi:10.1016/j.porgcoat.2019.04.064

32. Belmonte A, Guzmán D, Fernández-Francos X, la Flor SD. Effect of the network structure and programming temperature on the shape-memory response of thiol-epoxy "click" systems. *Polymers*. 2015;7:2146-2164. doi:10.3390/polym7101505

33. Petersen NJ, Nikolajsen RPH, Mogensen KB, Kutter JP. Effect of joule heating on efficiency and performance for microchip-based and capillary-based electrophoretic separation systems: a closer look. *Electrophoresis*. 2004;25:253-269. doi:10.1002/elps.200305747

34. Wang X, Sparkman J, Gou J. Electrical actuation and shape memory behavior of polyurethane composites incorporated with printed carbon nanotube layers. *Compos Sci Technol*. 2017;141:8-15. doi:10.1016/j.compscitech.2017.01.002

35. Zheng Y, Qin J, Shen J, Guo S. Controllable distribution of conductive particles in polymer blends via a bilayer structure design: a strategy to fabricate shape-memory composites with tunable electro-responsive properties. *J Mater Chem C*. 2020;8:9593-9601. doi:10.1039/D0TC01854F

36. Wang W, Liu D, Liu Y, Leng J, Bhattacharyya D. Electrical actuation properties of reduced graphene oxide paper/epoxy-based shape memory composites. *Compos Sci Technol*. 2015;106:20-24. doi:10.1016/j.compscitech.2014.10.016

37. Quadrini F, Iorio L, Bellisario D, Santo L. Shape memory polymer composite unit with embedded heater smart mater. *Structure*. 2021;30:75009. doi:10.1088/1361-665X/ac00cb

38. An Y, Okuzaki H. Novel electro-active shape memory polymers for soft actuators. *Jpn J Appl Phys*. 2020;59:61002. doi:10.35848/1347-4065/ab8e08